Tectonics®

RESEARCH ARTICLE
10.1029/2023TC008163

Mega-Folding of a Basement During Incipient Intra-Plate Continental Subduction (Alpine Central Iberia)

Rubén Díez Fernández[1], Gerardo de Vicente[2,3], Diana Moreno-Martín[3,4], Carlos Fernández[2,3], Ricardo Arenas[3,4], and Francisco J. Rubio Pascual[5]

[1]Departamento de Geología y Subsuelo, CN-IGME-CSIC, Unidad Territorial de Salamanca, Salamanca, Spain, [2]Departamento de Geodinámica, Estratigrafía y Paleontología, Facultad de Ciencias Geológicas, Universidad Complutense de Madrid, Madrid, Spain, [3]Instituto de Geociencias CSIC-UCM, Madrid, Spain, [4]Departamento de Mineralogía y Petrología, Universidad Complutense, Madrid, Spain, [5]Departamento de Geología y Subsuelo, CN-IGME-CSIC, Madrid, Spain

Abstract Metamorphic basements are usually considered rigid and isotropic at a large scale. However, basements contain inherited weaknesses that may potentially accommodate superimposed contraction (e.g., fault reactivation), and that favor fold nucleation (e.g., penetrative foliations). If these conditions are met, what could be the factors that impede the development of basement folds or their recognition? Actual basement folding is rarely documented, especially for large dimensions. Here we provide a case example, discussed from the perspective of structural analysis of surface data and sustained by geophysical data. The basement of the Spanish-Portuguese Central System is defined by an Alpine mega-fold (Hiendelaencina Antiform) that trends parallel to this mountain range and affects the basement and its sedimentary cover, collectively. The wavelength of this fold matches or even surpasses the thickness of the crust that hosts it (36–41 km). The Moho under this mega-fold is displaced by an Alpine fault that accounts for incipient intraplate continental subduction. The topography of the mantle may reflect an up-warping compatible with the mega-fold observed on the surface. Mega-folding is observed in the hanging wall of the Berzosa Fault, which emerges as a SE-dipping, Variscan (Paleozoic), extensional fault reactivated as a basal decollement upon Alpine (Cenozoic) contraction. The mega-fold was formed after well-oriented planar anisotropies in the basement (foliation and bedding). The development of this fold was assisted by heterogeneous shearing (coeval thrusting) plus the buttressing effect of pre-existing, near-vertical, crustal-scale faults (Somolinos and Somosierra), which inhibited slip-upsection through the basal decollement (Berzosa Fault).

Key Points:

- The basement of the easternmost part of the Spanish-Portuguese Central System is affected by an Alpine mega-fold
- The mega-fold has a wavelength that matches the thickness of the crust and is soled by a thrust that displaces the Moho
- Mega-folding occurred in a context of incipient intraplate subduction ruled by Variscan structural inheritance in the basement

Correspondence to:
R. Díez Fernández,
r.diez@igme.es

Citation:
Díez Fernández, R., de Vicente, G., Moreno-Martín, D., Fernández, C., Arenas, R., & Rubio Pascual, F. J. (2024). Mega-folding of a basement during incipient intra-plate continental subduction (Alpine Central Iberia). *Tectonics*, *43*, e2023TC008163. https://doi.org/10.1029/2023TC008163

Received 30 OCT 2023
Accepted 22 MAR 2024

Author Contributions:
Conceptualization: Rubén Díez Fernández, Gerardo de Vicente, Diana Moreno-Martín, Carlos Fernández, Francisco J. Rubio Pascual
Data curation: Rubén Díez Fernández, Gerardo de Vicente, Diana Moreno-Martín, Carlos Fernández
Formal analysis: Rubén Díez Fernández, Gerardo de Vicente, Diana Moreno-Martín, Carlos Fernández, Ricardo Arenas, Francisco J. Rubio Pascual
Funding acquisition: Rubén Díez Fernández, Francisco J. Rubio Pascual
Investigation: Rubén Díez Fernández, Gerardo de Vicente, Diana Moreno-Martín, Carlos Fernández, Ricardo Arenas, Francisco J. Rubio Pascual
Methodology: Rubén Díez Fernández
Project administration: Rubén Díez Fernández, Francisco J. Rubio Pascual

1. Introduction

In fold-thrust belts characterized by cold deformation (no metamorphism), there is a tendency to consider their basements as rigid and isotropic at a large scale. This is reflected in many cross-sections, especially those at the crustal-scale, which obliterate the structure of the basement, even when widely exposed, only drawing the cover structure.

In orogens containing a basement, there are some uncertainties about how deformation is distributed between the hard part (the basement) and the soft part (the sedimentary cover). In the absence of pre-existing weaknesses across the basement, its sedimentary cover requires less stress to be deformed and it may detach from the basement and be duplicated by thrusts (thin-skinned tectonics) (Calabrò et al., 2003; Chapple, 1978; Lacombe et al., 2003). If the basement contains inherited mechanical weaknesses (e.g., previous faults), these can rule how deformation is distributed (Brown et al., 2022; Butler et al., 2006; Holdsworth et al., 1997; Selander et al., 2012; Webb & Johnson, 2006). Accordingly, the orogens exhibit various deformation styles that range from pure thin- to pure thick-skinned tectonics (Pfiffner, 2017; Pfiffner et al., 2006).

Temperature affects the rheological behavior of the orogenic crust by softening the lithosphere, either if the temperature is inherited from a previous stage or the temperature increase is sourced directly from the orogenic building. In the internal zones of orogens, previous major faults (e.g., former suture zones) can be readily folded and reworked (not reactivated) under metamorphic conditions (Díez Fernández et al., 2019, 2022). In these cases, the basement and sedimentary cover may deform similarly. On the other hand, cold deformation conditions do not prevent folding at any scale in a sedimentary cover, but in the literature, folding appears challenging in cold basement rocks at a large scale (commonly treated as rigid blocks).

Resources: Rubén Díez Fernández
Validation: Rubén Díez Fernández, Ricardo Arenas, Francisco J. Rubio Pascual
Writing – original draft: Rubén Díez Fernández
Writing – review & editing: Gerardo de Vicente, Diana Moreno-Martín, Carlos Fernández, Ricardo Arenas, Francisco J. Rubio Pascual

There is a variety of mechanisms by which a sedimentary cover is folded while its underlying basement remains relatively unaffected by folds (see extended revision by Lacombe and Bellahsen (2016)). Strain distribution by fluid circulation and/or thermal weakening (Beaudoin et al., 2011; Bellahsen et al., 2012), or heterogeneous shearing (damage zones) ahead of fault tips (Bump, 2003; Erslev, 1986, 1991; García & Davis, 2004; Narr & Suppe, 1994) may confer a folded appearance to basements. In turn, the actual folding of a basement is hardly documented using outcropping structures (Bellahsen et al., 2016; García & Davis, 2004) and requires well-oriented planar anisotropies (e.g., penetrative foliations) (Schmidt et al., 1993).

The reactivation of pre-existing structures is a process that may involve pieces of basement and its cover into superimposed compressional deformation in thrust belts (e.g., Berberian, 1995; Brown et al., 1999, 2022; Granado et al., 2016; Horton & Folguera, 2022; Jackson, 1980; Lacombe & Mouthereau, 2002; Mitra & Mount, 1998; Mouthereau et al., 2002). The tendency to consider the basements as rigid objects, reluctant to be folded under cold conditions, relies on the few documented cases of cold basements affected by folds of significant scale, in various tectonic scenarios such as: the mega-antiforms in gneiss (thermal) domes (Teyssier & Whitney, 2002; Yin, 2004), the curved geometry of slabs (Mahadevan et al., 2010; Turcotte & Schubert, 2002), or in the oroclines (Carey, 1955; Johnston et al., 2013).

Metamorphic basements contain inherited weaknesses (e.g., faults) through which superimposed contraction can be accommodated. They also contain abundant planar anisotropies from which folds can be nucleated (e.g., bedding and penetrative foliations; Schmidt et al., 1993). Accordingly, the development of basement folds and their recognition seems, in our view, a multifaceted issue. On the one hand, the orientation of inherited faults relative to regional stress may not favor their reactivation and/or the shortening and folding of a foliated bedrock. If the orientation of inherited or newly formed faults is right, large faults could trigger large folds (e.g., Gerbault et al., 1999), depending on Moho temperatures, shortening rates (Schmalholz et al., 2009), and behavior of the mantle (Davy & Cobbold, 1991). However, the entire lithosphere can be affected by low-amplitude, large-wavelength folds (lithospheric folding), and so can the basements (e.g., Tikoff et al., 2022). On the other hand, the basements are typically multi-deformed, so the ascription of folds to a given deformation event is not a straightforward process. This problem can be solved by tracking the deformation in the cover, which should have a reflection in the basement. Here we discuss a case example based on extensive structural analysis of surface data and geophysical data. We provide evidence for mega-folding affecting collectively a basement and its cover, the wavelength of which is similar to, or even exceeds the thickness of the crust that hosts it. We discuss whether this mega-folding affects the entire crust, and the mechanisms, boundary conditions, and geodynamic setting behind it.

2. Geological Setting

The Spanish-Portuguese Central System (SPCS) and the Iberian Chain (IC) are intraplate orogens formed after the Cenozoic convergence between Iberia-Africa and Eurasia (de Vicente et al., 2007, 2018). The SPCS strikes E-W and NE-SW and is connected to the IC at the east, which strikes NW-SE (Figure 1a). The SPCS and IC comprise a sedimentary cover and basement cores. The basement cores were deformed and metamorphosed during the Variscan Orogeny (Díez Fernández et al., 2016; Fernández Rodríguez, 1991; González Lodeiro, 1980; Moreno-Martín et al., 2022; Rubio Pascual et al., 2013). The cover can be divided into pre-orogenic and syn-orogenic about the timing of the Alpine orogenesis. The Alpine pre-orogenic cover includes strata that span from the Permian to the Cretaceous (Paleocene) and were deposited in continental and marine environments established and expanded during continental rifting (López-Gómez et al., 2019; Sopeña et al., 1988). The Alpine syn-orogenic sediments were mainly deposited in endorheic Cenozoic continental basins (Alonso-Gavilán et al., 2004; Alonso-Zarza et al., 2004), the largest and widest of which occupy the forelands at both flanks of the mountain belts, namely the Madrid, Duero, Almazán, and Ebro Cenozoic basins (Figure 1b). The syn-orogenic cover is divided into sedimentary units bounded by discontinuities, that is, allostratigraphic units (UBS, Cunha et al., 2019; Figure 2). One of the main differences between SPCS and IC is the thickness of the pre-orogenic materials. Whereas the IC is an inverted rift formed during Alpine contraction, the thickness of the pre-orogenic cover is much lower in the eastern SPCS, with no evidence of previous extensional stages related to thermal subsidence in the rift flanks (de Vicente et al., 2009). The pre-orogenic sedimentary cover is missing to the west of the SPCS up to the Lusitanian Basin in Portugal. The Triassic Keuper facies serve as a detachment level in the IC, whereas in the SPCS, the sedimentary cover is attached to the basement with no detachments (de Vicente et al., 2018, 2022).

10.1029/2023TC008163

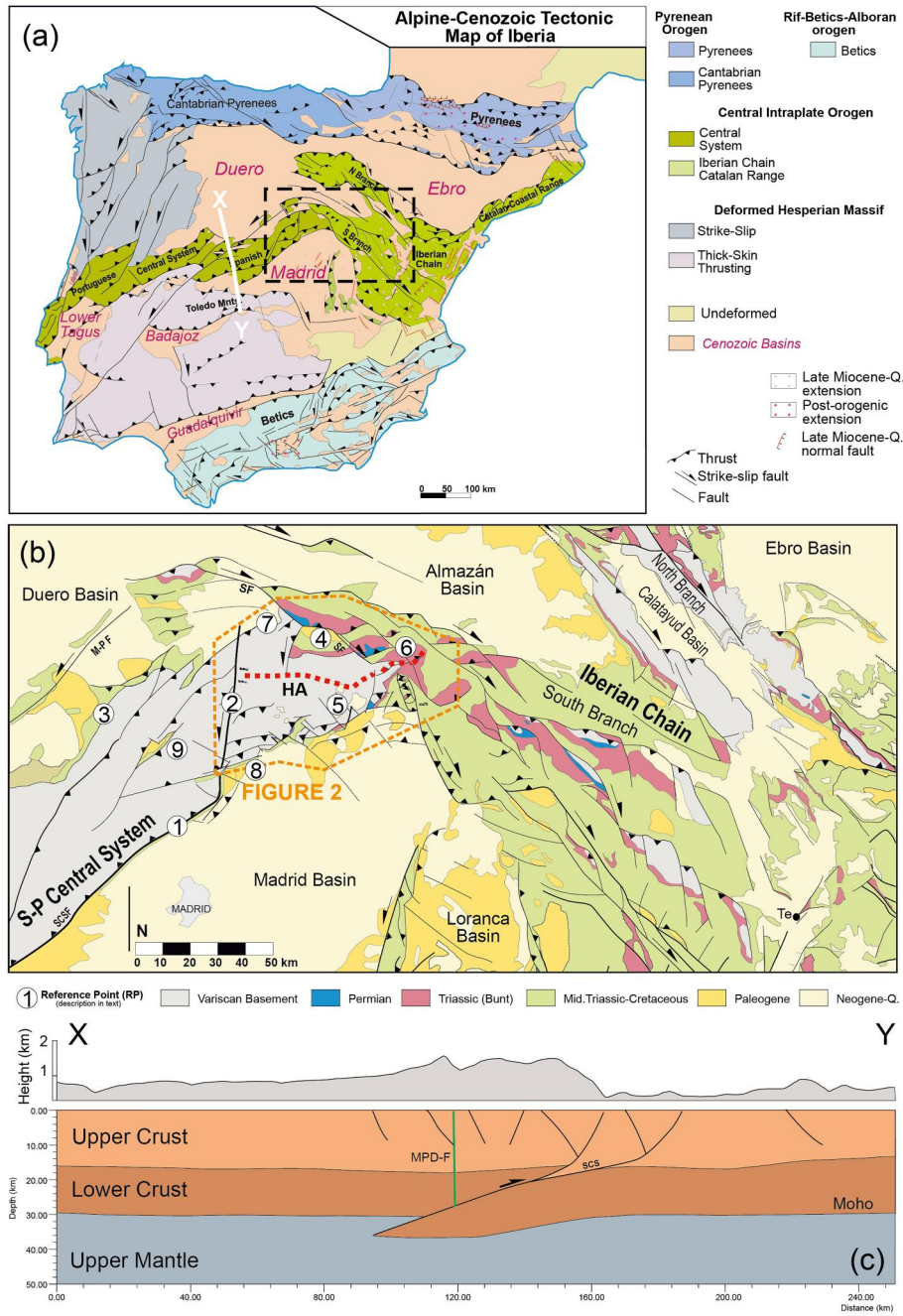

Figure 1. (a) Simplified Alpine Tectonic Map of Iberia. (b) Regional geology map of the Spanish-Portuguese Central System and the Iberian Chain focused on the elements related to its Alpine evolution, namely the main faults, the Variscan basement, the pre-orogenic cover (Permian—Cretaceous), and the syn-orogenic cover (Cenozoic). The location of the geological map in Figure 2 is indicated. Reference points (e.g., RP-1) are used to guide data presentation and interpretations in the main text. The red dashed line represents the axial trace of the Hiendelaencina Antiform. Abbreviations: HA—Hiendelaencina Antiform; M-PF—Messejana—Plasencia Fault; SCS—South Central System Thrust; SF—Somolinos Fault; SPF—Somosierra Pass Fault. (c) Profile from global-phase seismic interferometry (Andrés et al., 2019) crossing the Gredos Sector. MP D/F and SCS/SG are shown.

At a crustal-scale, the structure of the SPCS is an asymmetric pop-up flanked by thrusts to the NW and SE (de Vicente et al., 2018). The deformation concentrates in a single crustal thrust at the south (South Central System Thrust—SCS), in the Madrid Cenozoic Basin, whereas at the north (Duero Cenozoic Basin), the deformation is distributed through several faults. The Moho is displaced by the SCS, a S-directed thrust with a dip of ~30°

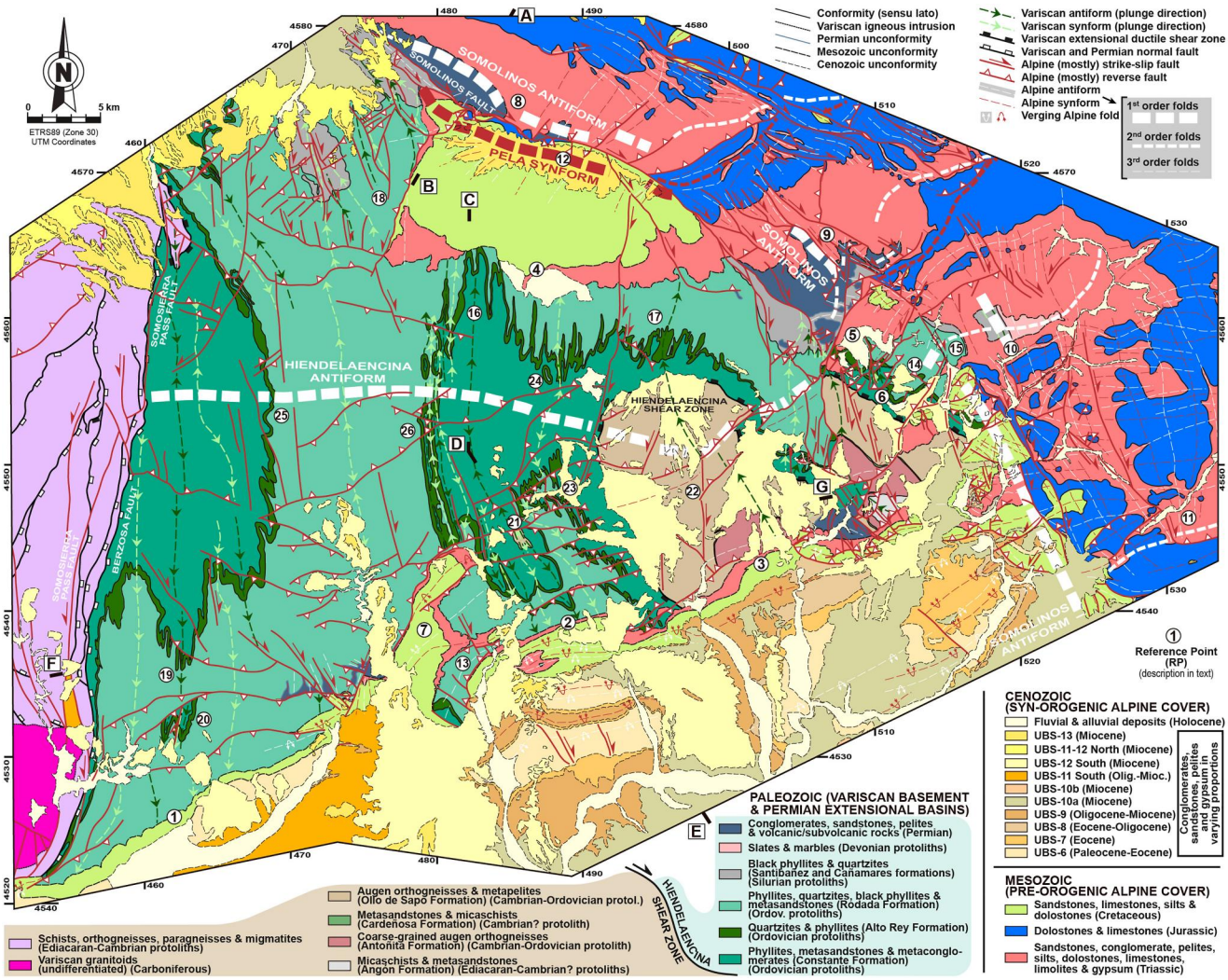

Figure 2. Geological map of the easternmost section of the Spanish-Portuguese Central System. Reference points (e.g., RP-1) are used to guide data presentation and interpretations in the main text. The map has been produced after our data and a compilation and synthesis of previous works (de Vicente et al., 2022; Fernández Rodríguez, 1991; González Lodeiro, 1980; Rubio Pascual, 2013).

(Andrés et al., 2019, 2020), which is connected to the emerging SE-directed thrust that bounds the SPCS northwest of Madrid city (RP-1; Figure 1b) (de Vicente et al., 2018). In its easternmost part, the southern section of the SPCS hosts numerous NW-directed (back)thrusts (e.g., de Vicente & Muñoz-Martín, 2013; González-Casado et al., 2002) that are considered to sole into a shallowly dipping inherited detachment (de Vicente et al., 2022), referred to as the Berzosa Fault (Escuder Viruete et al., 1998; Hernaiz Huerta et al., 1996; Rubio Pascual et al., 2013). This detachment is a reactivated Late Variscan—Permian normal fault that is thought to connect to a SE-directed crustal-scale thrust at depth (de Vicente et al., 2022).

The southern (Castilian) branch of the IC is a right lateral transpressional deformation belt that accommodates the uplift of the SPCS at a crustal-scale (de Vicente et al., 2009). Some sections of the IC may show a fold-and-thrust belt structure (Guimerà, 2018), but the Alpine thrusts co-exist with both left and right lateral strike-slip faults. The Somolinos Fault (SF in Figure 1b) is a steeply NE-dipping, right lateral strike-slip fault that separates the SPCS from the southern branch of the IC (Figure 1a). This fault was the main border fault during the Permo-Triassic rifting and was reactivated during the Mesozoic and Cenozoic. The Somolinos Fault belongs to the dextral strike-slip system that dominates the structure of the southern IC (Arche & López-Gómez, 1996; de Vicente et al., 2009). The Somosierra Pass Fault is a system of left-lateral strike-slip faults that separates the easternmost section of the SPCS from the rest of it (RP-2; Figure 1b). This system is connected to the emerging

major thrust that defines the southern boundary of the SPCS, that is, the SCS (RP-1; Figure 1b) (de Vicente et al., 2007).

The presence of lithospheric/crustal folds in Iberia was discussed by Cloetingh et al. (2002) and Fernández-Lozano et al. (2011), who argued that the timing of such folds is coincidental with upper crustal folds. Both can be explained by Cenozoic intraplate compression, likely assisted by the reactivation of inherited Variscan faults. Both types of folding (lithospheric and crustal) were deduced after Fourier analysis of the topography and Bouguer anomaly around Iberia (Muñoz-Martín et al., 2010). Alpine folds affecting the basement have been identified in the Iberian Chain (Liesa Carrera & Casas Sainz, 1994). In the SPCS, this folding has been identified at the micro- to mesoscale, mostly within the damage zones of Alpine faults (de Vicente, Muñoz-Martín, et al., 2021). The existence of larger Alpine folds in this basement was put forward by Moreno-Martín et al. (2022), who recognized that the basement and its cover were collectively affected by the same folds.

The basement of the SPCS mostly consists of metamorphic rocks (see extensive descriptions of its lithostratigraphy by González Lodeiro (1980), Fernández Rodríguez (1991), Rubio Pascual (2013), and Moreno-Martín et al. (2022)). The bedrock of this basement is divided into units according to the age of their protoliths and the nature of the rocks (Figure 2). The units of the basement are pre-orogenic concerning the Variscan Orogeny, except for the syn-orogenic Carboniferous granitoids.

The Variscan structure of the basement of the SPCS includes N-S trending folds and shallowly dipping shear zones. Early Variscan folds tend to be overturned and E-verging (Figures 3a and 3b), while the late Variscan folds are homoaxial and upright (González Lodeiro, 1981). The shear zones are divided into two types. The early shear zones are ductile and were formed after early Variscan folding events (Hiendelaencina Shear Zone; Fernández Rodríguez, 1991; Moreno-Martín et al., 2022; Rubio Pascual et al., 2013). The late shear zones are ductile-brittle and cut the late Variscan folds (Berzosa Fault; Escuder Viruete et al., 1998; Hernaiz Huerta et al., 1996; Rubio Pascual et al., 2013). Accordingly, Variscan folds and shear zones were formed in alternating stages of crustal thickening and thinning, respectively (Arango et al., 2013; Díez Fernández et al., 2013). Variscan deformation resulted in composite foliations, whose mineral assemblages and parageneses define a normal, telescoped metamorphic zonation. The Hiendelaencina Shear Zone is a top-to-the-SE ductile shear zone that divides the basement into two parts (Fernández Rodríguez, 1991). In the upper structural levels of the basement (hanging wall of the Hiendelaencina Shear Zone; see structural subdivision in the legend of Figure 2, and Figure 4a), the main fabric was formed under low-grade metamorphic conditions (greenschist facies), and it is an axial planar foliation related to early Variscan folding plus a local reworking of it upon late Variscan folding (Moreno-Martín et al., 2022). In the lower structural levels (footwall of the Hiendelaencina Shear Zone; Figure 2), the main foliation is parallel to the boundaries between units and was formed under mid- to high-grade metamorphic conditions (amphibolite to granulite facies; Rubio Pascual et al., 2013). This foliation results from the pervasive reworking of early Variscan foliations within the Hiendelaencina Shear Zone (Moreno-Martín et al., 2022).

3. The Hiendelaencina Antiform

Evidence about Alpine folding in the SPCS exists at all scales. A regional view of the distribution of the pre-orogenic cover suggests that the Mesozoic strata rim the basement to the NW (RP-3; Figure 1b) and to the SE (RP-1; Figure 1b). These strata continue to the E (RP-4-5; Figure 1b), up to converge and define the map pattern of a fold closure (RP-6; Figure 1b). This fold is a NE-plunging antiform, which will be referred to as the Hiendelaencina Antiform (HA).

The regional structure of the cover of the SPCS implies that the basement–cover interface is a folded unconformity, with a major SE-dipping fold limb located on the southeastern border of the basement (RP-1-2-3; Figure 2) (Figures 3a and 3c), and a major NNE-dipping limb on the northern border (RP-4-5; Figure 2) (Figures 3b and 3d). A zoom into the hinge zone defined by these two major fold limbs (RP-6; Figure 2) reveals several smaller folds affecting the cover (1–3 km in wavelength), and a set of SE-directed thrusts affecting both the cover and its basement. Deep within the regional exposure of the basement (RP-7; Figure 2), the Mesozoic sedimentary layer shows folding patterns that run parallel to the Alpine thrusts traversing the basement.

The Alpine folds that rotated the basement-cover unconformity trend ENE-WSW (Figure 4b). This trend is roughly parallel to the strike of the Alpine thrusts that affect the basement (Figure 2). The axis plunge of these

10.1029/2023TC008163

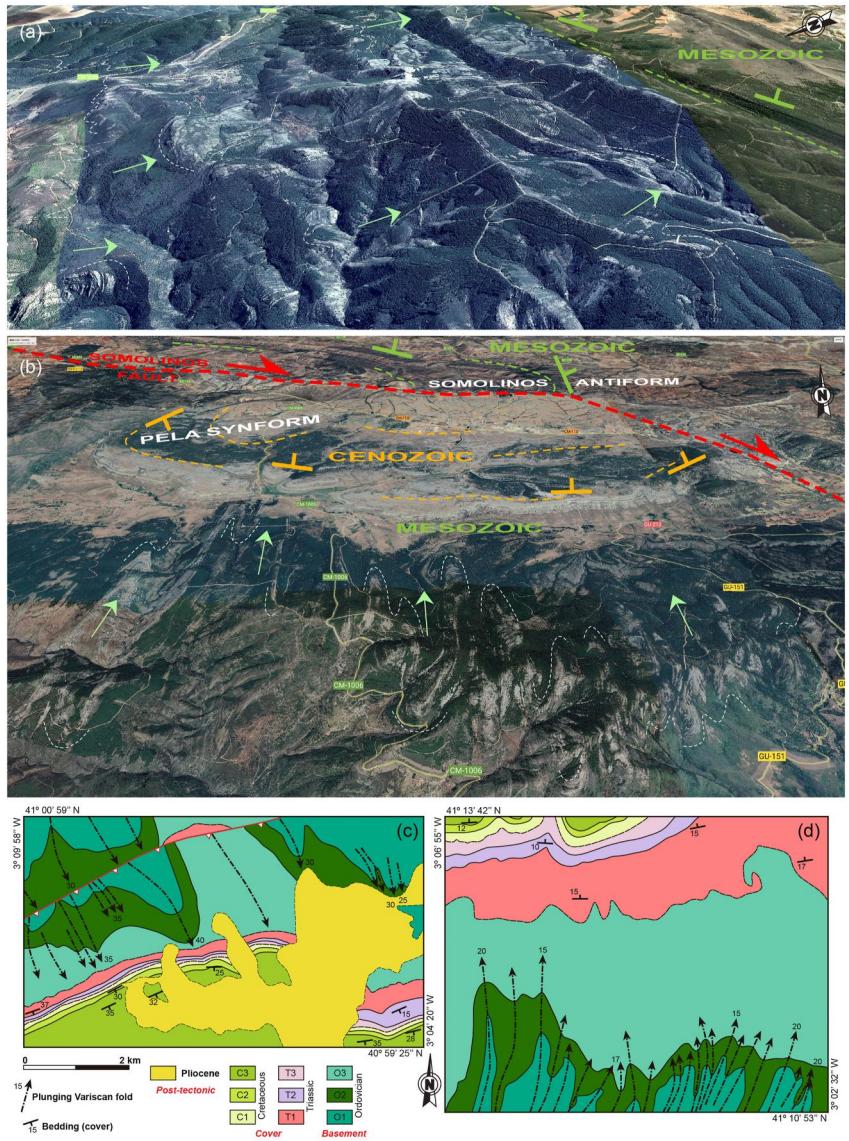

Figure 3. Aerial views of the two limbs of the Hiendelaencina Antiform (source: Google Earth), and geological maps of those areas. (a) The southern limb is defined by a S-dipping cover (Mesozoic) resting onto Paleozoic metamorphic rocks affected by S-plunging Variscan folds. Aerial view obtained from Reference Point 26 (Figure 2) looking at the SE. (b) The northern limb is defined by a cover (Mesozoic and Cenozoic) resting onto Paleozoic metamorphic rocks affected by N-plunging Variscan folds. The Cenozoic and Mesozoic strata are cut by the Somolinos Fault (red dashed line) and affected by the Pela synform and Somolinos antiform, respectively. Aerial view obtained from Reference Point 25 (Figure 2) looking at the NNE. Green arrows indicate the plunge direction of Variscan folds. White dashed lines show the local orientation of bedding in metamorphic rocks, while green and orange lines indicate the bedding in Mesozoic and Cenozoic strata, respectively. (c) Geological map of the aerial view represented in section (a). (d) Geological map of the aerial view represented in section (b).

folds varies locally between E- to W-plunging, although the termination of the basement exposure to the east (major fold closure) indicates a regional E-plunging of the Alpine folds.

The cover includes abundant Jurassic strata to the north and east of the Somolinos Fault (within the Iberian Chain). In this section, there exist two families of Alpine folds. One family is parallel to the right lateral strike-slip faults that run across this part of the Iberian Chain, while the other family trends almost perpendicular to the former and parallel to the Alpine thrusts of the SPCS. Alpine thrusts and strike-slip faults are believed to have formed simultaneously in a transpressional context (de Vicente et al., 2009). The family of thrust-parallel folds

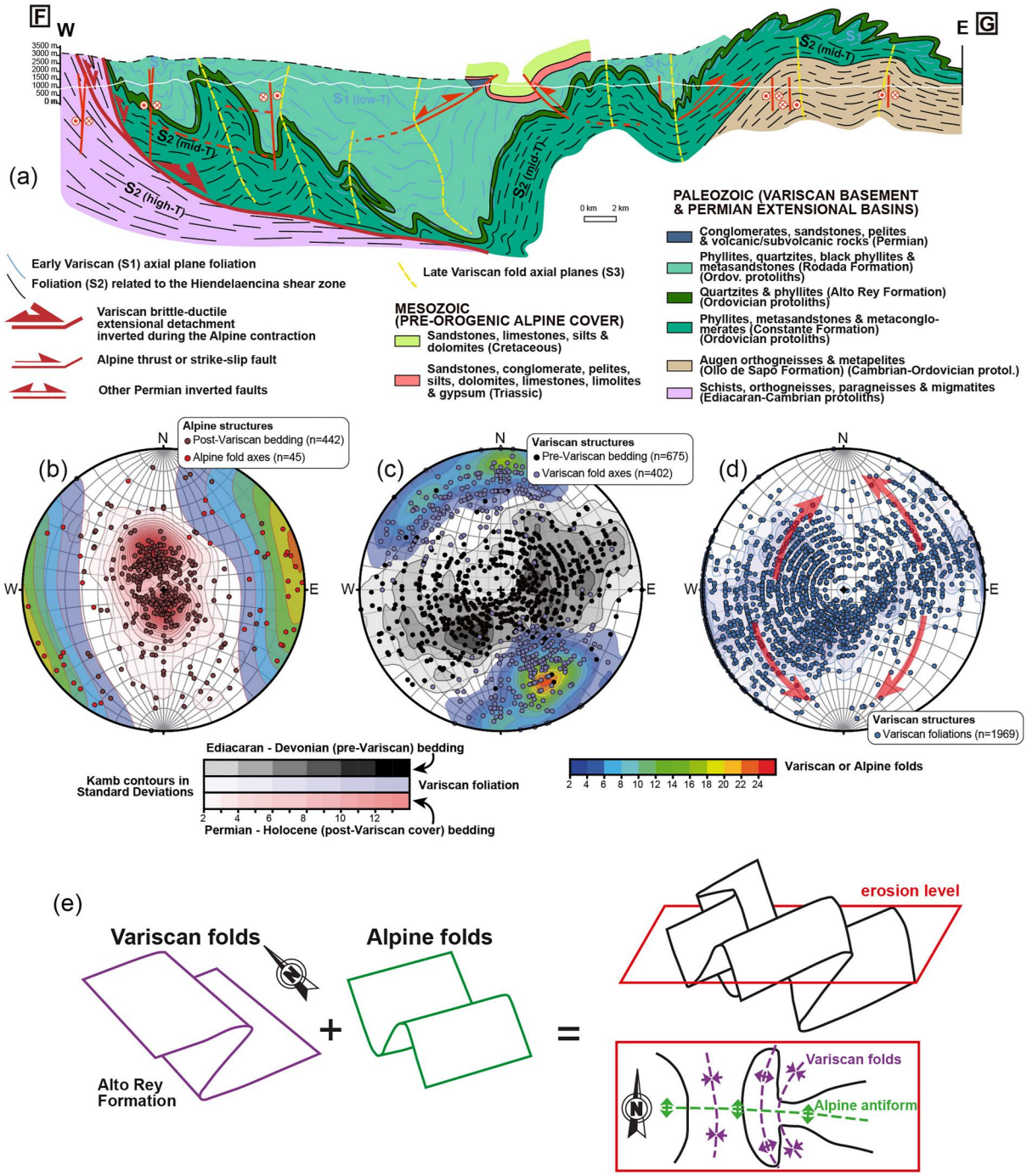

Figure 4. (a) Cross-section showing the structure of the basement (see trace in Figure 2; after Rubio Pascual, 2013; de Vicente et al., 2022). (b) Stereoplot showing the orientation of the bedding of the sedimentary cover (poles to S_0; Permian—Cenozoic strata) and of the axes of Alpine folds (measured directly in the field). (c) Stereoplot showing the orientation of the bedding of the basement rocks (poles to S_0; Ediacaran—Devonian strata) and of the axes of Variscan folds (field observation). (d) Stereoplot showing the orientation of the poles to Variscan foliations of the basement rocks. Many poles define an E-W to WSW-ENE girdle typical for planes affected by N-S trending folds, such as the Variscan ones. The rest of the poles occur along the hypothetical orientations toward which the poles of a primary WSW-ENE girdle would be reoriented (red arrows) if affected by E-W trending folds, such as the Alpine ones. (e) Idealized sketch showing the large-scale type-2 interference pattern between the N-S-trending, E-verging Variscan folds and the E-W trending Alpine folds. The Alto Rey Formation is illustrated as the reference level (modified from Ramsay (1967)). A hypothetical horizontal section yields a cartographic geometry very similar to that shown in Figure 2. α and β angles (Ramsay, 1967) are ~90° and range between 0°–45°, respectively. The shallower the dip of the Variscan fold axial planes, the lower is β. If $\alpha = 90°$, intermediate values of β (Variscan folds range between upright and overturned) will result in a fold interference straddling type-1 and type-2 patterns. Accordingly, the main interference pattern is type-2 (mushroom-like), but there are some type-1 examples (dome and basin; e.g., RP-24-26 in Figure 2).

includes several major E- to NE-plunging antiforms (RP-8-9-10-11; Figure 2). The Permian and Triassic strata of these folds are exposed along a lineament that connects regional fold culminations and is parallel to the Somolinos Fault, if slightly oriented counterclockwise from that fault. At a regional scale, this lineament can be observed as an open NW-SE trending antiform, a fold closure of which occurs next to the Somolinos Fault (RP-8; Figure 2). Accordingly, this fold will be referred to as the Somolinos Antiform (Figure 3b). The Pela Synform is intersected by the NW-SE Somolinos Fault, in a E-W restraining step (RP-12; Figure 2) filled by Oligocene—Lower Miocene syn-orogenic sediments drawing a progressive unconformity. This synform separates the Somolinos Antiform from the Hiendelaencina Antiform (Figure 3b). Individually, the Pela Synform, the Somolinos Antiform, and the Hiendelaencina Antiform are asymmetric and south-verging (*sensu lato*). Their forelimbs are either steeper than their backlimbs or they are missing (cut) and replaced by a N-dipping fault. For instance, the cover in the southern limb of the Pela Synform is nearly horizontal, while the dip in its northern limb and the southern limb of the Hiendelaencina Antiform is higher than 25°, sometimes including inverted strata. In the case of the Somolinos Antiform, its (southern) forelimb is mostly cut by the (NE-dipping) Somolinos Fault (Figure 3b).

In some sections, the core of an antiform defined by the sedimentary cover matches the core of an antiform defined by units from the basement (RP-13; Figure 2). This is also the case of fold closures defined by Ordovician (RP-14; Figure 2), Silurian (RP-15; Figure 2), Devonian (RP-10; Figure 2), and Triassic (RP-15; Figure 2) strata alike (see further analysis by Moreno-Martín et al. (2022)). Accordingly, both the cover and basement are collectively affected by Alpine folds.

The bedrock map of the SPCS basement reveals N-S to NW-SE trending folds at various scales (Figures 2 and 4c) (Figures 3a and 3b). These folds are accompanied by axial plane foliation and were formed during superimposed Variscan crustal thickening events (Fernández Rodríguez, 1991; González Lodeiro, 1981; Moreno-Martín et al., 2022; Rubio Pascual et al., 2013). The poles to regional Variscan foliation plot within a NE-SW trending girdle (Figure 4d). This pattern is expected for fabrics that are either axial planar to NW-SE trending folds and for fabrics that are affected by folds with that trend. However, part of those poles also approaches an N-S trending girdle (note path indicated by red arrows in Figure 4d), which is an orientation related to E-W trending folds.

At the micro-to mesoscale, the plunge of Variscan fold axes changes frequently from N- to S-plunging (Figures 2 and 4c). At the regional scale, only one major change is observed. This change divides the basement into two parts: a northern part featured by Variscan antiforms that close to the north (e.g., RP-16-17-18; Figure 2) (Figure 3b), and a southern part with the same folds closing to the south (e.g., RP-2-19; Figure 2) (Figure 3a). The quartzites of the Alto Rey Formation (Ordovician) depict an unequivocal fold interference map pattern that results from the combination between N-S and E-W trending folds (Figure 2). The giant mushroom-like (type-2) fold interference coexists with (type-1) structural domes (e.g., RP-20-21-22; Figure 2) and basins (e.g., RP-23-24; Figure 2). The median line of the giant mushroom coincides with the regional division between N- and S-plunging Variscan folds. This line aligns with the axial trace of the Hiendelaencina Antiform, that is, it is located at a similar distance from the exposures of Mesozoic strata located to the N and S of the basement. Around the giant mushroom interference drawn by the Alto Rey Formation, the base of the Mesozoic strata occupies similar position respect to the Variscan fold closures defined by that formation, either if Variscan folds plunge to the N (RP-16; Figure 2) or S (RP-2; Figure 2). This can only be achieved if the regional plunge of Variscan folds was essentially horizontal before the Mesozoic cover was deposited. Accordingly, the giant mushroom-like pattern emerged from the interference between Variscan folds occurring at various scales and a regional antiform that affected both the Mesozoic strata and the entire basement (Figure 4e). This major Alpine fold is the Hiendelaencina Antiform (Figures 1 and 2). This Alpine fold can also be identified by the curved pattern defined by the limbs of similarly large Variscan folds, which exhibit a map trace convex-to-the-E (RP-25; Figure 2) or -W (RP-26; Figure 2) depending on their primary E- or W-dipping geometry related to Variscan folds, respectively.

4. Crustal Structure of the Spanish-Portuguese Central System

Recent seismic studies indicate that the SCS passes through the entire crust and cuts off the Moho (Andrés et al., 2019, 2020; DeFelipe et al., 2022). The studied seismic section is located to the west of the Hiendelaencina Dome, but the SCS crops out up to the Madrid meridian. Further east, the SCS develops a tectonic wedge where only back-thrusts continue limiting the northern border of the Madrid Cenozoic Basin. Therefore, the SCS is the base of the wedge and continues up to the IC for more than 300 km.

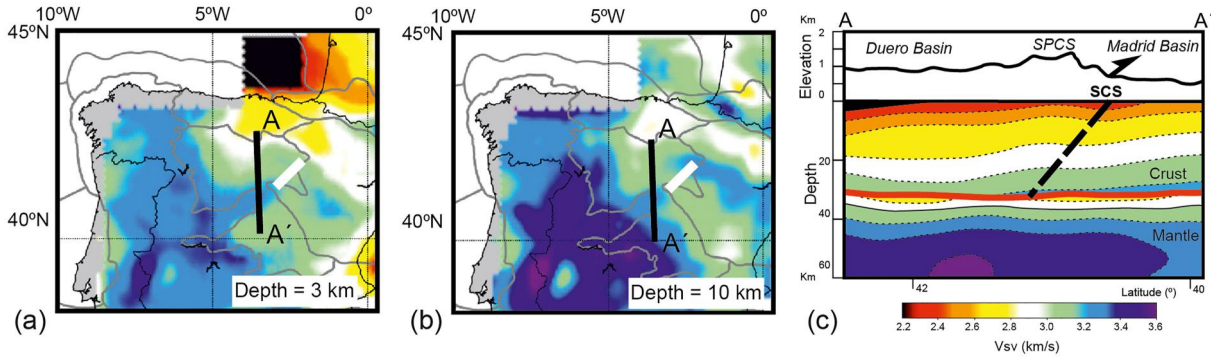

Figure 5. V_{sv} slices in the Iberian crust at sample depths of (a) 3 and (b) 10 km (central-depth ±3 km), along with a (c) vertical V_{sv} cross-section going through A-A′ (Feng & Diaz, 2023). Note the location of the South Central System Thrust (SCS) and the open antiformal structure that occurs on top of it.

Lower crustal ductile flow, along with its duplication as an effect of this crustal thrust, leads to a crustal thickening below the SPCS, which was deduced early from gravimetric studies (Suriñach & Vegas, 1988). From the combination of controlled-source seismic profiling and receiver functions, Diaz et al. (2016) drew a 3D Moho depth map of the Iberian Peninsula with a grid spacing of around 50 km. For the SPCS the deduced Moho depths range between 36 and 41 km, whereas in the adjacent Duero and Madrid Cenozoic Basins, the crustal thickness varies between 32 and 35 km. Nevertheless, the map does not have adequate resolution to detect crustal folds with a wavelength of a few tens of km as the one here deduced. Recently, a shear velocity model of the crust and uppermost mantle has been developed for Iberia (Feng & Diaz, 2023). In the study area, the V_{sv} crustal model outlines an open antiform visible in the 3 and 10 km depth maps (Figures 5a and 5b), also observed in cross-section (Figure 5c), with higher V_{sv} in the SPCS close to the surface than in the surrounding areas.

5. Crustal-Scale Model and Kinematics

The Alpine upper crust structure of the eastern SPCS is defined by a mega-fold (Hiendelaencina Antiform) located at the hanging wall of the SCS. This fold is bounded to the NE and W by right and left lateral brittle shear zones, the Somolinos and Somosierra Pass faults, respectively. The steepness of the latter faults, together with the gently NW-dipping geometry of the SCS, define an orogenic wedge cored by the Hiendelaencina Antiform (Figure 6). Both the Somolinos and Somosierra Pass fault zones serve as tectonic boundaries, partitioning Alpine strain into components: orogen-normal and orogen-parallel/oblique. The normal component was accommodated by thrusts and major folds (e.g., SCS and Hiendelaencina Antiform), while the parallel component is distributed through right and left lateral faults (e.g., Somolinos and Somosierra Pass faults). In the western part of the SPCS, the transition from sections dominated by tectonic transport directed to the SE (pro-wedge) to others with transport to the NW (retro-wedge) occurs within the SPCS (de Vicente et al., 2018). In the eastern section of the SPCS, this transition occurs within the southern branch of the Iberian Chain (de Vicente et al., 2009).

Alpine deformation partitioning was not the result of decomposing oblique convergence (e.g., Platt, 1993). It would have rather been determined by the structural inheritance of the basement. The Somolinos Fault is a reactivated Permian-Triassic fault, and so seems the case for the Somosierra Pass Fault, which is largely parallel to the trace of the Variscan Berzosa Fault (Figure 2). Accordingly, the orientation of these faults is independent of the Alpine stresses and represented readily crustal rheological weaknesses upon Alpine deformation. The obliqueness of their inherited traces forces the wedging of the basement to the north (RP-7; Figure 1b). The steepness and strike of the Somolinos and Somosierra Pass faults seem to have conferred a virtual buttress role to the combination of both, thus forcing lateral tectonic escape in response to local indentation. Accordingly, these two faults would have contributed to diminishing the N-directed propagation of the Alpine shortening through the upper crust by transforming N-S compression into lateral sliding of fault blocks to the SE (e.g., right-lateral sliding in the Iberian Chain; de Vicente et al., 2009) and to the SW (e.g., left-lateral movement of the Messejana-Plasencia Fault; de Vicente, Olaiz, et al., 2021). Collectively, the three major Alpine folds of the easternmost part of the SPCS (Hiendelaencina, Pela, Somolinos) define a S-verging train of folds. This regional asymmetry is likely connected to the N-dipping geometry of the underlying SCS. However, the spacing of these major folds is closer in the vicinity of the Somolinos Fault, thus reflecting that Alpine shortening was

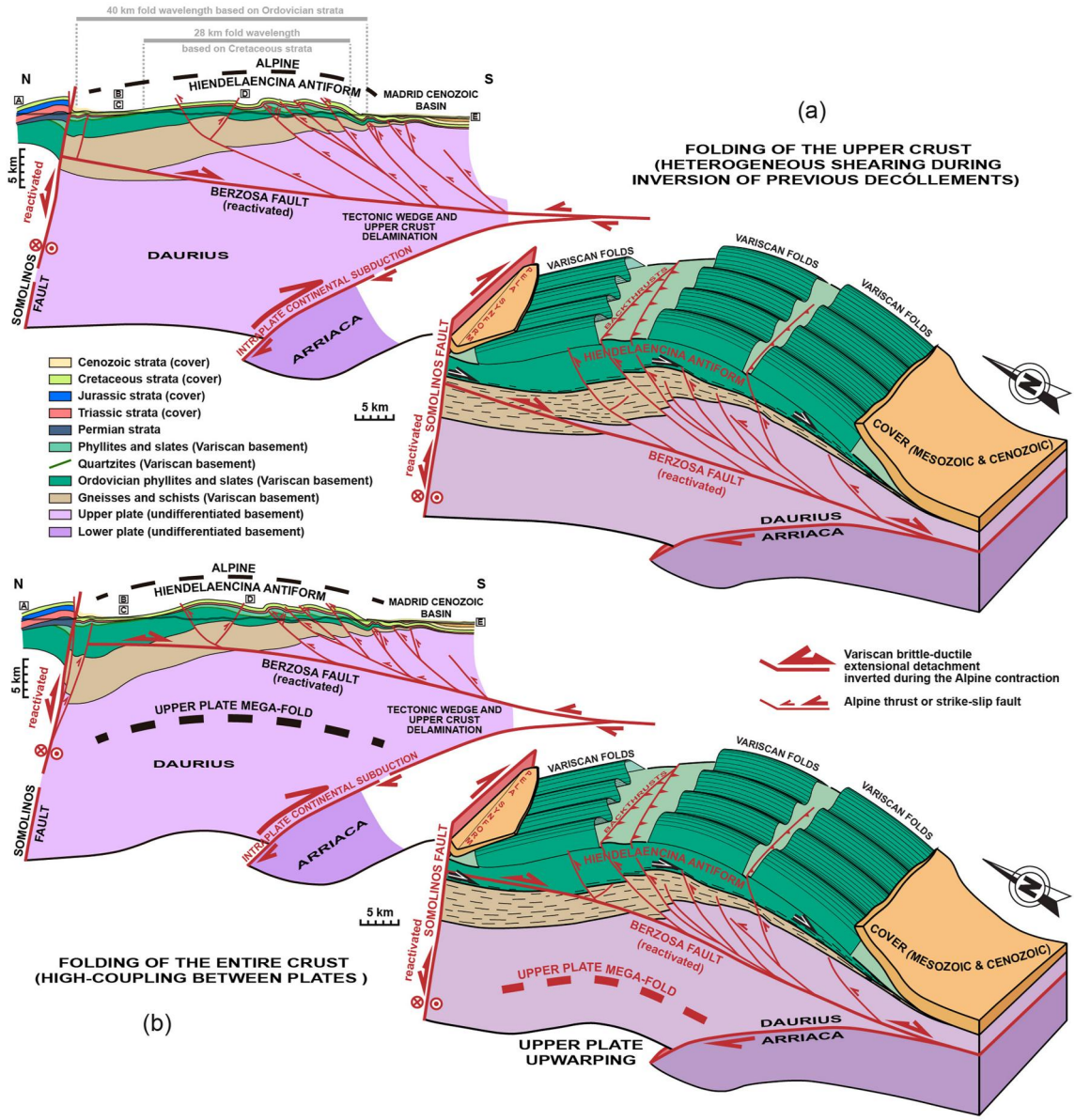

Figure 6. Crustal-scale, composite cross-sections of the easternmost part of the Spanish-Portuguese Central System (based on the map of Figure 2), and 3D schematic models that explain the development of the Hiendelaencina Antiform is a context of intra-plate subduction. The cross-sections are focused on the Alpine structures. The upper third of the cross-sections is supported by surface geology. Letters A through E refer to points used to trace the cross-section (see location in Figure 2). (a) Cross section and 3D model that consider that the Hiendelaencina mega-fold is restricted to the (reactivated) hanging wall of the Berzosa Fault. (b) Cross-section and 3D model that consider that the Hiendelaencina mega-fold affects the entire crust. Both models include (back)thrust imbricates that branch off from the Berzosa Fault a cut its hanging wall. Some imbricates may also represent Permian normal faults inverted upon Alpine contraction. In model 6a, the Alpine shortening in the upper crust could be greater than in model 6b, where shortening is more distributed. In model 6b, the Hiendelaencina Antiform affects the whole crust and, eventually, the Berzosa Fault, which may not have been fully inverted (note that in the uppermost section of this fault, the Permian extension has not been overcome by Alpine shortening; Figure 2).

preferentially accumulated in this section, probably due to the buttress effect of that fault. Within the Iberian Chain, the family of Alpine folds parallel to the right lateral strike-slip faults reflects a similar effect, which suggests that N-S compression was also transmitted into the buttress.

The Hiendelaencina Antiform is constrained by three crustal-scale faults. The minimum wavelength of the Hiendelaencina Antiform ranges between 28 km (if measured in Cretaceous strata) and 40 km (if estimated from Ordovician strata) (Figure 6a); therefore, it approaches, even surpasses the thickness of the crust in the region (36–41 km; Diaz et al., 2016). The wavelength of the Hiendelaencina Antiform needs a mechanism(s) able to curve

(upwarp) a significant portion of the crust. However, the question remains as to whether this fold impacts the entire crust or only a segment of it.

5.1. Upper Crust Folding

The bedding and foliations that define the internal structure of the basement affected by the Hiendelaencina Antiform represent well-oriented planar anisotropies from which the fold nucleates (e.g., Bellahsen et al., 2016). Some of the characteristics of mode 2 folds described by Schmidt et al. (1993) are met: (a) basement deformation occurs in a broad zone; (b) cover strata are not significantly thinned through the fold; (c) the axial plane penetrates the basement; (d) there are back-thrusts; (e) the basement consists of well-foliated rocks. Accordingly, the mechanisms based on strain distribution and heterogeneous shearing proposed to fold basements in thrust fold belts (see revision by Lacombe and Bellahsen (2016)) would explain the development of the Hiendelaencina Antiform if this is a fold restricted to an upper section of the crust.

The Berzosa Fault represents the largest mechanical weakness in the region. This fault juxtaposes two crustal sections with contrasting rheological properties, that is, an upper block mostly consisting of slates and phyllites, and a lower block made of gneisses and minor granitoids (Rubio Pascual et al., 2013). The Alpine Somosierra Pass Fault mimics the trace of the Berzosa Fault (Figure 2), indicating the Alpine reactivation of the uppermost structural sections of the latter. The set of NW-directed (back)thrusts that cut across the Hiendelaencina Antiform branches off from an underlying crustal detachment that should extend beneath the entire basement of the eastern SPCS (de Vicente et al., 2022). The SE-dipping geometry of those Alpine (back)thrusts fits the geometry of the Variscan Berzosa Fault at depth (Escuder Viruete et al., 1998; Hernaiz Huerta et al., 1996; Rubio Pascual et al., 2013), if slightly steeper. This way, the folding of the basement could have been assisted by heterogeneous shearing distributed along reactivated (Berzosa) and/or newly formed faults (Figure 6a). We think that the collection of minor Alpine folds affecting the basement reflects heterogeneous shearing along local faults (de Vicente, Muñoz-Martín, et al., 2021). However, given that the Hiendelaencina Antiform matches the magnitude of the Berzosa Fault, with tens of km in wavelength and length, respectively, the origin of the Hiendelaencina Antiform should be related to shearing along a larger fault, such as the Berzosa Fault. In this model, the buttress effect of the Somolinos and Somosierra Pass faults would have inhibited slip along the Berzosa Fault, thus contributing to the shortening and folding of the rocks in its hanging wall (e.g., buttress folds; Abu Sharib et al., 2017; Baum et al., 2008; Withjack et al., 2010).

5.2. Modeling of the Alpine Mega-Fold

The shortening of the upper crust to generate a mega-fold is a process that can be evaluated, at least in a first approximation, using a simple mechanical model. In this model, the upper crust acts as a competent layer subjected to shortening parallel to its limiting surfaces (i.e., to buckling), due to the buttressing effect mentioned above. The model will also serve to discuss the possible presence of a decoupling level at the base of the competent folding level, which could correspond to the Berzosa Fault, as indicated above in this work.

The strength of the continental lithosphere in the SPCS and the adjacent Madrid Basin has been analyzed by various authors (e.g., Gómez-Ortiz et al., 2005; Ruiz et al., 2006; Tesauro et al., 2009). Figure 7a shows two of the strength envelopes from Jiménez-Díaz et al. (2012) that provide very valuable information to understand the mechanical behavior of the continental lithosphere in the eastern part of the SPCS during the Alpine Orogeny. The crustal structure in these profiles has been obtained from seismic data (e.g., Banda et al., 1981; Suriñach & Vegas, 1988; see Jiménez-Díaz et al., 2012 for more information on the construction of the profiles). An essential result of Jiménez-Díaz et al.'s (2012) calculations is the difference in the total strength of the lithosphere (T_{ils}, which in the cited article is named S_{max}). The integrated stress in the Madrid Basin is almost twice that of the SPCS due to a higher level of stress in both the lithospheric mantle and the upper crust. This difference explains the greater deformability of the SPCS lithosphere concerning the Madrid Basin. It is also important to highlight that the upper crust, about 11 km thick in the SPCS, is the only lithospheric level that exhibits brittle deformation.

According to the SPCS rheological profile, to apply a folding model to that lithosphere or part of it, it is not possible to simply use the classic viscous folding model of Biot (1957) and Ramberg (1961). Burov and Cloetingh (2009) have pointed out that, for the folding of the lithosphere as a whole and considering Newtonian media, the dominant wavelength predicted by the Biot-Ramberg model can be up to an order of magnitude higher than that observed. An alternative considered by Burov and Cloetingh (2009) was that of a stiff viscous layer at the top

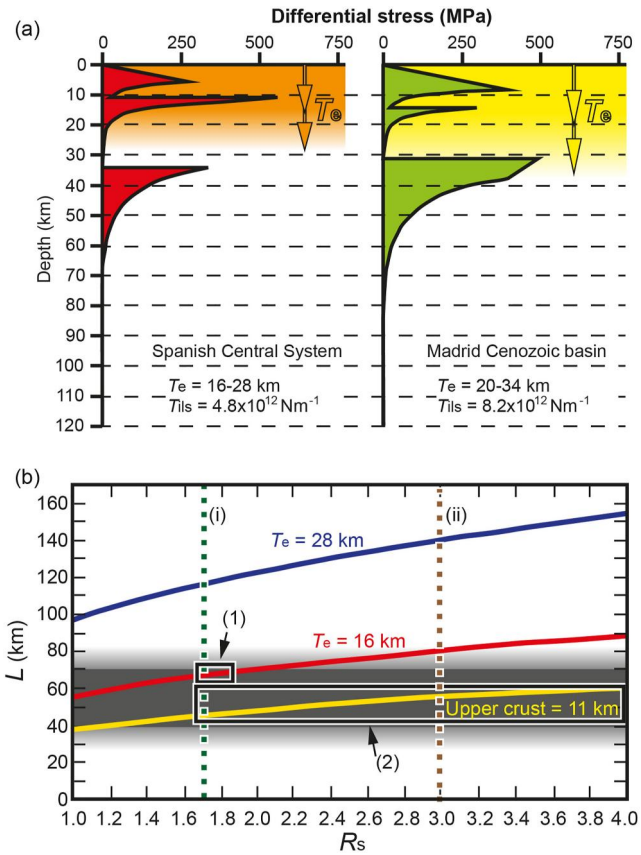

Figure 7. (a) Rheological profiles by Jiménez-Díaz et al. (2012) for the SPCS and the Madrid Basin. The values of the thermal and mechanical parameters selected to obtain these profiles are presented and discussed in Jiménez-Díaz et al. (2012), who also indicate the results of the elastic thickness (T_e, shaded areas) and the total integrated lithospheric strength (T_{ils}). (b) Results of the calculation of the mega-fold wavelength (L) for a range of ratios of elastic shear moduli (R_s) and for distinct thicknesses of the competent layer (given by the effective elastic thickness –T_e- of the SPCS -16 and 28 km- according to Jiménez-Díaz et al., 2012, and by the thickness of the upper crust: 11 km). (i) and (ii) indicate the minimum R_s values for deformation of elastoplastic material (1.7, according to So et al. (2012)), and for folding of an elastic competent layer (3, according to Price and Cosgrove (1990)). Rectangles (1) and (2) mark the predictions of the model compatible with the observed wavelength of the Hiendelaencina mega-fold (gray shaded area). See the main text for an explanation.

of an inviscid medium, subjected to the action of gravity. In this work, a simpler approach has been chosen based on the indication of Biot (1957) and Ramberg (1961) in the sense that their well-known equation for the dominant wavelength (L) of a single layer subjected to buckling could also be expressed in terms of the ratio (R_s) of elastic shear moduli of the layer and its matrix (see also Price and Cosgrove (1990)):

$$L = 2\pi a(R_s/6)^{1/3}, \quad (1)$$

where a is the thickness of the competent layer.

To semi-quantitatively determine the wavelength of the large crustal folds in the SPCS, it is suggested here to use estimates of the elastic thickness of the lithosphere (T_e) as a proxy for the thickness of the competent layer (a). According to Watts and Burov (2003), T_e describes the effective flexural rigidity and is associated with the integral depth of the bending stress. Therefore, it does not exactly coincide with the thickness of an elastic layer subjected to buckling, hence we consider that this is only a first approach to the problem. Jiménez-Díaz et al. (2012) offer T_e values of the studied area which, in the case of the SPCS, would vary between 18 km (wet rheology) and 28 km (dry rheology). Other determinations of T_e in the SPCS, such as that of Tesauro et al. (2009), show lower values, equal to or less than 10 km, which practically coincides with the thickness of the upper crust (Figure 7a). In this way, three values of "a" have been considered in this work: 11, 16 and 28 km. Price and Cosgrove (1990) suggest that values of R_s between 3 and 10 can reasonably reproduce values of L/a obtained from real folds in nature. So et al. (2012) have found, based on the study of numerical models simulating elastoplastic rheologies, that deformations and the development of mechanical instabilities can be observed in materials with shear modulus contrasts of $R_s > 1.7$. In this way, a range of values of $R_s > 1$ has been considered, with special interest in $R_s > 1.7$ and >3.

The wavelength (L) of the Hiendelaencina mega-fold exceeds 28 km and most likely also 40 km (see above). Figure 2 shows that in the western part of the studied area, this wavelength is greater than 50 km. The upper limit is unknown because the structure is covered by Cenozoic materials to the north (Duero Basin) and south (Madrid Basin). But, according to the sections shown in Figure 6, it could be greater than 70 km. Therefore, the results of the folding model (Equation 1) have been checked with a wide range of L values between 28 and 80 km (gray shaded area in Figure 7b), although values between 40 and 70 km are considered much more probable. The wavelength predicted by the folding model for the greatest thickness of the competent layer (a: $T_e = 28$ km) exceeds 100 km (Figure 7b), making it unable to explain the observed folds. In the case of the intermediate thickness for the competent layer (a: $T_e = 16$ km) folds with reasonable wavelengths ($L \approx 65$–70 km) are obtained for values of R_s between 1.7 and 1.9 (rectangle 1 in Figure 7b), but too long wavelengths are predicted ($L > 80$ km) when $R_s > 3$, that is, in the most suitable conditions to generate buckling folds according to Price and Cosgrove (1990). Finally, if the competent layer is limited to the upper crust (a: 11 km), it is possible to obtain folds with wavelengths compatible with those of the Hiendelaencina mega-fold for a very wide range of R_s values (rectangle 2 in Figure 7b). Thus, when $R_s = 1.7$, L is 45 km, while when $4 > R_s > 3$, L stabilizes between 55 and 60 km.

In conclusion, the classical competent layer buckling model (Equation 1) can predict upper crustal folds whose wavelength mimics that of the Hiendelaencina mega-fold. While it would be possible to derive wavelength values from a layer whose thickness aligns with a wet crust model (elastic thickness of 16 km; Jiménez-Díaz et al., 2012), the likelier explanation is that the Hiendelaencina mega-fold resulted from the folding of the upper crust (a:

11 km). In this sense, it is important to recall that, according to Watts and Burov (2003), T_e is not necessarily associated with the thickness of a competent layer but includes contributions from the brittle and ductile parts of the entire lithosphere as a whole. This result coincides with those of the 2D models and 3D flexure models of the SPCS and the Madrid Cenozoic Basin by Van Wees et al. (1996), who noted a low effective elastic thickness and a partial decoupling of upper and lower crustal deformation.

The contact between the upper crust and the middle crust, whose depth (11 km) has been obtained from seismic information, is characterized by a pronounced relative strength minimum (Figure 7a). It is important to note that a perfect correspondence is not expected between the block diagrams of Figure 6, which represent geological units (most with similar rheological behaviors), and the strength profiles of Figure 7a. However, the strength minimum approximately coincides with the average position at depth of the Berzosa Fault as determined from surface geological information and depicted in Figure 6. Therefore, this contact combines the presence of an ancient Variscan structure, susceptible to being reactivated, with that of a minimum in the mechanical strength of the crust. Thus, it could have acted as a level of decoupling between the upper crust and the rest of the lithosphere during Alpine shortening.

5.3. Folding of the Entire Crust

In the study area, the Moho depth defines a relative minimum of ∼36 km in a region where the thickness of the surrounding crust reaches ∼41 km (Diaz et al., 2016); therefore, the topography of the Moho is compatible with an open crustal antiform. The V_{sv} crustal model should be compliant with the deduced geometry of the SCS at depth, but no significant crustal thickening is observed. Accordingly, the V_{sv} crustal model is better fitted with a crustal fold developed over the Berzosa Fault. However, when considering the depth to which the antiform extends within the crust (almost to the base of the crust; Figure 5c), it cannot be ruled out that the entire crust is folded.

Strong plate coupling in subduction zones can produce open crustal folds in the upper plate (note the open antiform in close-to-the-trench sections; e.g., Bottrill et al., 2012; Gvirtzman & Stern, 2004; Regalla et al., 2010). In a continental collision, this type of folds can also be produced under conditions of strong coupling along the plate boundary (Luth et al., 2010). The SCS and its prolongation to the NE into the study area has been recently imaged as a crustal-scale thrust that displaces the Moho and produces a crustal imbrication (Andrés et al., 2019, 2020) that mimics an incipient continental subduction zone (de Vicente et al., 2022). In this scenario, the mechanical coupling between "plates" (Daurius and Arriaca; two pieces of regular continental crust) is expected to be strong; therefore, the movement of the lower plate could have dragged the section of the upper plate closer to the "trench" down. The resulting structure in the upper plate would be an asymmetric antiform verging toward the lower plate, that is, to the SE (Figure 6b). This is essentially the large-scale Alpine structure of the study area, and, in a broad sense, accounts for the topographic upwarping of the hanging wall to the SCS along the SPCS (DeFelipe et al., 2022).

The Hiendelaencina Antiform could, at least partially, be the expression of an upper plate antiform (Figure 6b). This mechanism does not invalidate, but may be added to, the mechanisms based on heterogeneous shearing, reactivation, and buttressing (Section 5.1). The low resolution of the Moho topography in the eastern SPCS does not allow us to quantify the contribution of each mechanism to the global architecture of the crust in the study area.

Analyzing the folding of the entire crust or lithosphere involves examining how different layers with varying vertical and horizontal rheologies behave, which determines the coupling or decoupling between these layers. This analysis can be conducted using lithospheric-scale analog or numerical modeling (e.g., Auzemery et al., 2021; Cloetingh et al., 2002; Martinod & Davy, 1994; McAdoo & Sandwell, 1985; Sokoutis et al., 2005). These models are even capable of predicting the generation of disharmonic or polyharmonic folds with different dominant wavelengths depending on the geometric, thermal and mechanical structure of the lithosphere. Such type of approach is used to obtain the characteristics of folds that only affect the upper crust, the entire crust or even the lithosphere as a whole. Some initial work in this line has already been advanced, on a large scale, in Iberia (e.g., Cloetingh et al., 2002), but it would be necessary to address similar studies in more detail in the SPCS, which is beyond the scope of this work. However, analog modeling experiments indicate that weak layers enhance strain localization. The wavelength of lithospheric/crustal folding depends primarily on its stratification and rheology. A weak mantle produces folding wavelengths between 60 and 165 km (Sokoutis et al., 2005). Short (40–70 km) and intermediate (75–90 km) wavelengths are found in many orogens and have been explained as

strong upper crust and strong lower crust respectively (e.g., Delvaux et al., 2013). The Hiendelaencina antiform can be considered a case with a short wavelength, which may indicate a strong upper crust and a strong lower crust. In the light of the discussion presented here, obtaining a more detailed profile of the Moho and a subsurface image of the Berzosa Fault are key milestones not only to understanding the evolution of this Alpine intraplate orogen but to quantifying the actual shortening accumulated in this region and the structures and mechanisms that led the process.

6. Conclusions

Basements can be affected by folds at any scale and should not be treated as rigid and isotropic on a large scale. The basement of the Spanish-Portuguese Central System has undergone deformation into an Alpine mega-fold with a wavelength that reaches or even exceeds the thickness of the continental crust. The local structure of the Moho exhibits an up-warping compatible with this mega-fold and is also disrupted by a reverse fault that leaves this fold on top. Mega-folding occurred in the hanging wall (upper plate) of an incipient intraplate continental subduction zone. Folding might have been a result of the high coupling between the upper and lower plate (drag effect over the upper plate), yet it was assisted by heterogeneous shearing during the Cenozoic inversion of Permian-Triassic faults that existed in the upper plate. The buttressing effect of pre-existing, near-vertical, crustal-scale faults (Somolinos and Somosierra) inhibited slip upsection through a basal decollement (Berzosa Fault), thus favoring fold amplification.

Detecting basement mega-folds might prove challenging due to the complexity of distinguishing them from the primary deformation structures of the basement. However, identifying these folds allows studying the contribution of folding to the rising of mountain belts. Intraplate orogens can be constructed by folding the whole crust; or a significant part of it. This process is favored by inherited crustal faults, which would represent low-yielding layers to accommodate the superimposed shortening through the basement instead of its cover. We believe that the primary geometry of reactivated faults makes a fundamental difference in intraplate orogens. If shortening is transmitted through near-vertical faults, reactivation would allow for strike-slip tectonics. If such faults were shallowly dipping and penetrated the crust, shortening can be transmitted into the fault blocks and generate low-plunging folds at the expense of large pieces of crust or the whole crust (i.e., including the Moho).

Data Availability Statement

The structural data [Dataset] used for analysis in the study are available at Mendeley Data via https://doi.org/10.17632/83ffn959js.1, with CC BY 4.0 license (Díez Fernández, 2023).

Acknowledgments
We are thankful for the constructive revisions provided by Ernst Willingshofer, Antoine Auzemery, and Pablo Granado. This publication is part of projects PID2020-112489GB-C22 and PID2020-112489GB-C21, funded by MCIN/AEI/10.13039/501100011033.

References

Abu Sharib, A. S. A. A., Abdel-Fattah, M. M., Salama, Y. F., & Abdel-Gawad, G. I. (2017). Extension-related buttress-like folds, the western side of the Gulf of Suez rift, Egypt. *International Journal of Earth Sciences*, *106*(7), 2527–2547. https://doi.org/10.1007/s00531-017-1445-1

Alonso-Gavilán, G., Armenteros, I., Carballeira, J., Corrochano, A., Huerta, P., & Rodríguez, J. M. (2004). Cuenca del Duero. In J. A. Vera (Ed.), *Geología de España* (pp. 550–556).

Alonso-Zarza, A. M., Calvo, J. P., Silva, P. G., & Torres-Ruiz, T. (2004). Cuenca del Tajo. In J. A. Vera (Ed.), *Geología de España* (pp. 556–561).

Andrés, J., Ayarza, P., Schimmel, M., Palomeras, I., Ruiz, M., & Carbonell, R. (2020). What can seismic noise tell us about the Alpine reactivation of the Iberian Massif? An example in the Iberian Central System. *Solid Earth*, *11*(6), 2499–2513. https://doi.org/10.5194/se-11-2499-2020

Andrés, J., Draganov, D., Schimmel, M., Ayarza, P., Palomeras, I., Ruiz, M., & Carbonell, R. (2019). Lithospheric image of the Central Iberian Zone (Iberian Massif) using global-phase seismic interferometry. *Solid Earth*, *10*(6), 1937–1950. https://doi.org/10.5194/se-10-1937-2019

Arango, C., Díez Fernández, R., & Arenas, R. (2013). Large-scale flat-lying isoclinal folding in extending lithosphere: Santa María de la Alameda dome (Central Iberian Massif, Spain). *Lithosphere*, *5*, 483–500. https://doi.org/10.1130/l270.1

Arche, A., & López-Gómez, J. (1996). Origin of the Permian-Triassic Iberian Basin, central-eastern Spain. *Tectonophysics*, *266*(1), 443–464. https://doi.org/10.1016/s0040-1951(96)00202-8

Auzemery, A., Willingshofer, E., Sokoutis, D., Brun, J. P., & Cloetingh, S. A. (2021). Passive margin inversion controlled by stability of the mantle lithosphere. *Tectonophysics*, *817*, 229042. https://doi.org/10.1016/j.tecto.2021.229042

Banda, E., Suriñach, E., Aparicio, A., Sierra, J., & Ruiz de la Parte, E. (1981). Crust and upper mantle structure of the central Iberian Meseta (Spain). *Geophysical Journal of the Royal Astronomical Society*, *67*(3), 779–789. https://doi.org/10.1111/j.1365-246x.1981.tb06954.x

Baum, M. S., Withjack, M. O., & Schlische, R. W. (2008). The ins and outs of buttress folds: Examples from the Fundy rift basin, Nova Scotia and New Brunswick, Canada. In D. E. Brown (Ed.), *Central Atlantic conjugate margins, program and extended abstracts* (pp. 53–61). Dalhousie University.

Beaudoin, N., Bellahsen, N., Lacombe, O., & Emmanuel, L. (2011). Fracture-controlled paleohydrogeology in a basement-cored, fault-related fold: Sheep Mountain Anticline, Wyoming, United States. *Geochemistry, Geophysics, Geosystems*, *12*(6). https://doi.org/10.1029/2010gc003494

Bellahsen, N., Jolivet, L., Lacombe, O., Bellanger, M., Boutoux, A., Garcia, S., et al. (2012). Mechanisms of margin inversion in the external Western Alps: Implications for crustal rheology. *Tectonophysics*, *560–561*, 62–83. https://doi.org/10.1016/j.tecto.2012.06.022

Bellahsen, N., Sebrier, M., & Siame, L. (2016). Crustal shortening at the Sierra Pie de Palo (Sierras Pampeanas, Argentina): Near-surface basement folding and thrusting. *Geological Magazine*, *153*(5–6), 992–1012. https://doi.org/10.1017/s0016756816000467

Berberian, M. (1995). Master "blind" thrust faults hidden under the Zagros folds: Active basement tectonics and surface morphotectonics. *Tectonophysics*, *241*(3–4), 193–224. https://doi.org/10.1016/0040-1951(94)00185-c

Biot, M. A. (1957). Folding instability of a layered viscoelastic medium under compression. *Proceedings of the Royal Society of London*, *A242*, 444–454.

Bottrill, A. D., van Hunen, J., & Allen, M. B. (2012). Insight into collision zone dynamics from topography: Numerical modelling results and observations. *Solid Earth*, *3*(2), 387–399. https://doi.org/10.5194/se-3-387-2012

Brown, D., Alvarez-Marron, J., Camanni, G., Biete, C., Kuo-Chen, H., & Wu, Y. M. (2022). Structure of the south-central Taiwan fold-and-thrust belt: Testing the viability of the model. *Earth-Science Reviews*, *231*, 104094. https://doi.org/10.1016/j.earscirev.2022.104094

Brown, D., Alvarez-Marron, J., Perez-Estaun, A., Puchkov, V., & Ayala, C. (1999). Basement influence on foreland thrust and fold belt development: An example from the southern Urals. *Tectonophysics*, *308*(4), 459–472. https://doi.org/10.1016/s0040-1951(99)00147-x

Bump, A. P. (2003). Reactivation, trishear modeling and folded basement in Laramide uplifts: Implications for the origins of intracontinental faults. *Geological Society of America Today*, *13*(3), 4–10. https://doi.org/10.1130/1052-5173(2003)013<0004:rtmafb>2.0.co;2

Burov, E., & Cloetingh, S. (2009). Controls of mantle plumes and lithospheric folding on modes of intraplate continental tectonics: Differences and similarities. *Geophysical Journal International*, *178*(3), 1691–1722. https://doi.org/10.1111/j.1365-246x.2009.04238.x

Butler, R. W. H., Tavarnelli, E., & Grasso, M. (2006). Structural inheritance in mountain belts: An Alpine–Apennine perspective. *Journal of Structural Geology*, *28*(11), 1893–1908. https://doi.org/10.1016/j.jsg.2006.09.006

Calabrò, R. A., Corrado, S., Di Bucci, D., Robustini, P., & Tornaghi, M. (2003). Thin-skinned vs. thick- skinned tectonics in the Matese Massif, central-southern Apennines. *Tectonophysics*, *337*(3–4), 269–297. https://doi.org/10.1016/j.tecto.2003.09.010

Carey, S. W. (1955). The orocline concept in geotectonics. In *Papers and Proceedings of the Royal Society of Tasmania* (Vol. 89, pp. 255–288).

Chapple, W. M. (1978). Mechanics of thin-skinned fold-and-thrust belts. *Geological Society of America Bulletin*, *89*(8), 1189–1198. https://doi.org/10.1130/0016-7606(1978)89<1189:motfb>2.0.co;2

Cloetingh, S., Burov, E., Beekman, F., Andeweg, B., Andriessen, P. A. M., Garcia-Castellanos, D., et al. (2002). Lithospheric folding in Iberia. *Tectonics*, *21*(5), 1041–1067. https://doi.org/10.1029/2001tc901031

Cunha, P. P., de Vicente, G., & Martín-González, F. (2019). Chapter 5—Cenozoic sedimentation along the piedmonts of thrust related basement ranges and strike- slip deformation belts of the Iberian Variscan Massif. In C. Quesada & J. T. Oliveira (Eds.), *The geology of Iberia: A geodynamic approach*, *Regional geology reviews* (Vol. 4, pp. 131–165). Springer International Publishing.

Davy, P., & Cobbold, P. R. (1991). Experiments on shortening of a 4-layer model of the continental lithosphere. *Tectonophysics*, *188*(1), 1–25. https://doi.org/10.1016/0040-1951(91)90311-f

DeFelipe, I., Ayarza, P., Palomeras, I., Ruiz, M., Andrés, J., Alcalde, J., et al. (2022). Crustal imbrication in an alpine intraplate mountain range: A wide-angle cross-section across the Spanish-Portuguese central system. *Tectonics*, *41*(7), e2021TC007143. https://doi.org/10.1029/2021tc007143

Delvaux, D., Cloetingh, S., Beekman, F., Sokoutis, D., Burov, E., Buslov, M. M., & Abdrakhmatov, K. E. (2013). Basin evolution in a folding lithosphere: Altai–Sayan and Tien Shan belts in Central Asia. *Tectonophysics*, *602*, 194–222. https://doi.org/10.1016/j.tecto.2013.01.010

de Vicente, G., Cunha, P. P., Muñoz-Martín, A., Cloetingh, S. A. P. L., Olaiz, A., & Vegas, R. (2018). The Spanish-Portuguese central system: An example of intense intraplate deformation and strain partitioning. *Tectonics*, *37*(12), 4444–4469. https://doi.org/10.1029/2018tc005204

de Vicente, G., Díez Fernández, R., Olaiz, A., & Muñoz-Martín, A. (2022). Variscan inheritance induces Alpine upper crustal delamination in East Spanish–Portuguese Central System. *Tectonics*, *41*(8), e2022TC007315. https://doi.org/10.1029/2022tc007315

de Vicente, G., & Muñoz-Martín, A. (2013). The Madrid Basin and the central system: A tectonostratigraphic analysis from 2D seismic lines. *Tectonophysics*, *602*, 259–285. https://doi.org/10.1016/j.tecto.2012.04.003

de Vicente, G., Muñoz-Martín, A., Díez Fernández, R., & Olaiz, A. (2021). Kink bands alpinos en rocas foliadas del basamento varisco del Sistema Central. *Geogaceta*, *69*, 7–10. https://doi.org/10.55407/geogaceta102340

de Vicente, G., Olaiz, A., Muñoz-Martín, A., & Cunha, P. P. (2021). Longest and still longer: The Messejana-Plasencia dyke and its links with later Alpine deformation belt in Iberia. *Tectonophysics*, *815*, 229009. https://doi.org/10.1016/j.tecto.2021.229009

de Vicente, G., Vegas, R., Muñoz Martín, A., Silva, P. G., Andriessen, P., Cloetingh, S., et al. (2007). Cenozoic thick-skinned deformation and topography evolution of the Spanish Central System. *Global and Planetary Change*, *58*(1–4), 335–381. https://doi.org/10.1016/j.gloplacha.2006.11.042

de Vicente, G., Vegas, R., Muñoz-Martín, A., Van Wees, J. D., Casas-Sáinz, A., Sopeña, A., et al. (2009). Oblique strain partitioning and transpression on an inverted rift: The Castilian Branch of the Iberian Chain. *Tectonophysics*, *470*(3), 224–242. https://doi.org/10.1016/j.tecto.2008.11.003

Diaz, J., Gallart, J., & Carbonell, R. (2016). Moho topography beneath the Iberian-Western Mediterranean region mapped from controlled-source and natural seismicity surveys. *Tectonophysics*, *692*, 74–85. https://doi.org/10.1016/j.tecto.2016.08.023

Díez Fernández, R. (2023). Structural data from east Spanish-Portuguese central system [Dataset]. *Mendeley Data, V1*. https://doi.org/10.17632/83ffn959js.1

Díez Fernández, R., Arenas, R., Pereira, M. F., Sánchez Martínez, S., Albert, R., Martín Parra, L. M., et al. (2016). Tectonic evolution of Variscan Iberia: Gondwana—Laurussia collision revisited. *Earth-Science Reviews*, *162*, 269–292. https://doi.org/10.1016/j.earscirev.2016.08.002

Díez Fernández, R., Arenas, R., Rojo-Pérez, E., Sánchez Martínez, S., & Fuenlabrada, J. M. (2022). Tectonostratigraphy of the Mérida Massif reveals a new Cadomian suture zone exposure in Gondwana (SW Iberia). *International Geology Review*, *64*(3), 405–424. https://doi.org/10.1080/00206814.2020.1858355

Díez Fernández, R., Gómez Barreiro, J., Martínez Catalán, J. R., & Ayarza, P. (2013). Crustal thickening and attenuation as revealed by regional fold interference patterns: Ciudad Rodrigo basement area (Salamanca, Spain). *Journal of Structural Geology*, *46*, 115–128. https://doi.org/10.1016/j.jsg.2012.09.017

Díez Fernández, R., Jiménez-Díaz, A., Arenas, R., Pereira, M. F., & Fernández-Suárez, J. (2019). Ediacaran obduction of a fore-arc ophiolite in SW Iberia: A turning point in the evolving geodynamic setting of Peri-Gondwana. *Tectonics*, *38*(1), 95–119. https://doi.org/10.1029/2018tc005224

Erslev, E. A. (1986). Basement balancing of Rocky Mountain foreland uplifts. *Geology*, *14*(3), 259–262. https://doi.org/10.1130/0091-7613(1986)14<259:bbormf>2.0.co;2

Erslev, E. A. (1991). Trishear fault-propagation folding. *Geology*, *19*(6), 617–620. https://doi.org/10.1130/0091-7613(1991)019<0617:tfpf>2.3.co;2

Escuder Viruete, J., Hernáiz Huerta, P. P., Valverde-Vaquero, P., Rodríguez Fernández, R., & Dunning, G. (1998). Variscan syncollisional extension in the Iberian Massif: Structural, metamorphic and geochronological evidence from the Somosierra sector of the Sierra de Guadarrama (Central Iberian Zone, Spain). *Tectonophysics*, *290*(1–2), 87–109. https://doi.org/10.1016/s0040-1951(98)00014-6

Feng, L., & Diaz, J. (2023). A high-resolution shear velocity model of the crust and uppermost mantle beneath Westernmost Mediterranean including radial anisotropy. *Journal of Geophysical Research: Solid Earth*, *128*(9), e2023JB026868. https://doi.org/10.1029/2023jb026868

Fernández-Lozano, J., Sokoutis, D., Willingshofer, E., Cloetingh, S., & De Vicente, G. (2011). Cenozoic deformation of Iberia: A model for intraplate mountain building and basin development based on analogue modeling. *Tectonics*, *30*(1), TC1001. https://doi.org/10.1029/2010tc002719

Fernández Rodríguez, C. (1991). *Estudio de los procesos de deformación en la zona de Cizalla de Hiendelaencina (Sistema Central Español)* PhD Thesis (p. 522). Universidad Complutense.

García, P. E., & Davis, G. H. (2004). Evidence and mechanisms for folding of granite, Sierra de Hualfín basement-cored uplift, northwest Argentina. *AAPG Bulletin*, *88*(9), 1255–1276. https://doi.org/10.1306/04290403092

Gerbault, M., Burov, E. B., Poliakov, A. N. B., & Daignières, M. (1999). Do faults trigger folding in the lithosphere? *Geophysical Research Letters*, *26*(2), 271–274. https://doi.org/10.1029/1998gl900293

Gómez-Ortiz, D., Tejero, R., Ruiz, J., Babín-Vich, R., & González-Casado, J. M. (2005). Estimating the effective elastic thickness of the Iberian Peninsula's lithosphere based on multitaper spectral analysis. *Geophysical Journal International*, *160*(2), 729–735. https://doi.org/10.1111/j.1365-246x.2004.02499.x

González-Casado, J. M., Gumiel, P., Segura, M., & Giner, J. (2002). Estructuras compresivas en el Cretácico de Patones (Borde sur del Sistema Central Español, Prov. de Madrid). *Geogaceta*, *32*, 323–326.

González Lodeiro, F. (1980). *Estudio geológico estructural de la terminación oriental de la Sierra del Guadarrama (Sistema Central Español)* (p. 325). University of Salamanca.

González Lodeiro, F. (1981). La estructura del anticlinorio del Ollo de Sapo en la región de Hiendelaencina (extremo oriental del Sistema Central Español). *Cuadernos de Geologia Iberica*, *7*, 535–545.

Granado, P., Thöny, W., Carrera, N., Gratzer, O., Strauss, P., & Muñoz, J. A. (2016). Basement-involved reactivation in foreland fold-and-thrust belts: The Alpine–Carpathian Junction (Austria). *Geological Magazine*, *153*(5–6), 1110–1135. https://doi.org/10.1017/s0016756816000066

Guimerà, J. (2018). Structure of an intraplate fold-and-thrust belt: The Iberian Chain. A synthesis. *Geológica Acta*, *16*(4), 427–438.

Gvirtzman, Z., & Stern, R. J. (2004). Bathymetry of Mariana trench-arc system and formation of the Challenger Deep as a consequence of weak plate coupling. *Tectonics*, *23*(2), TC2011. https://doi.org/10.1029/2003tc001581

Hernaiz Huerta, P. P., Escuder Viruete, J. E., Rodríguez Fernández, L. R., Valverde Vaquero, P., & Dunning, G. (1996). Evolución estructural de la zona de cizalla extensional de Berzosa-Riaza, sector de Somosierra, Sistema Central Español. *Geogaceta*, *20*, 875–878.

Holdsworth, R. E., Butler, C. A., & Roberts, A. M. (1997). The recognition of reactivation during continental deformation. *Journal of the Geological Society*, *154*(1), 73–78. https://doi.org/10.1144/gsjgs.154.1.0073

Horton, B. K., & Folguera, A. (2022). Chapter 1 - tectonic inheritance and structural styles in the Andean fold-thrust belt and foreland basin. In G. Zamora & A. Mora (Eds.), *Andean structural styles* (pp. 3–28). Elsevier. https://doi.org/10.1016/B978-0-323-85175-6.00001-8

Jackson, J. A. (1980). Reactivation of basement faults and crustal shortening in orogenic belts. *Nature*, *283*(5745), 343–346. https://doi.org/10.1038/283343a0

Jiménez-Díaz, A., Ruiz, J., Villaseca, C., Tejero, R., & Capote, R. (2012). The thermal state and strength of the lithosphere in the Spanish Central System and Tajo Basin from crustal heat production and thermal isostasy. *Journal of Geodynamics*, *58*, 29–37. https://doi.org/10.1016/j.jog.2012.01.005

Johnston, S. T., Weil, A. B., & Gutiérrez-Alonso, G. (2013). Oroclines: Thick and thin. *GSA Bulletin*, *125*(5–6), 643–663. https://doi.org/10.1130/b30765.1

Lacombe, O., & Bellahsen, N. (2016). Thick-skinned tectonics and basement-involved fold–thrust belts: Insights from selected Cenozoic orogens. *Geological Magazine*, *153*(5–6), 763–810. https://doi.org/10.1017/s0016756816000078

Lacombe, O., & Mouthereau, F. (2002). Basement-involved shortening and deep detachment tectonics in forelands of orogens: Insights from recent collision belts (Taiwan, Western Alps, Pyrenees). *Tectonics*, *21*(4), 12-1–12-22. https://doi.org/10.1029/2001tc901018

Lacombe, O., Mouthereau, F., Angelier, J., Chu, H.-T., & Lee, J.-C. (2003). Frontal curvature and oblique ramp development at an oblique ramp development at an obliquely collided irregular margin: Geometry and kinematics of the NW Taiwan fold-thrust belt. *Tectonics*, *22*(3), 1025. https://doi.org/10.1029/2002tc001436

Liesa Carrera, C. I., & Casas Sainz, A. M. (1994). Reactivación alpina de pliegues y fallas del zócalo hercínico de la Cordillera Ibérica: Ejemplos de la Sierra de la Demanda y la Serranía de Cuenca. *Cadernos do Laboratorio Xeolóxico de Laxe*, *19*, 119–135.

López-Gómez, J., Alonso-Azcárate, J., Arche, A., Arribas, J., Fernández Barrenechea, J., Borruel-Abadía, V., et al. (2019). Permian-triassic rifting stage. In C. Quesada & J. T. Oliveira (Eds.), *The geology of Iberia: A geodynamic approach: Volume 3: The Alpine Cycle* (pp. 29–112). Springer International Publishing.

Luth, S., Willingshofer, E., Sokoutis, D., & Cloetingh, S. (2010). Analogue modelling of continental collision: Influence of plate coupling on mantle lithosphere subduction, crustal deformation and surface topography. *Tectonophysics*, *484*(1), 87–102. https://doi.org/10.1016/j.tecto.2009.08.043

Mahadevan, L., Bendick, R., & Liang, H. (2010). Why subduction zones are curved. *Tectonics*, *29*(6). https://doi.org/10.1029/2010tc002720

Martinod, J., & Davy, P. (1994). Periodic instabilities during compression of the lithosphere: 2. Analogue experiments. *Journal of Geophysical Research*, *99*(B6), 12057–12069. https://doi.org/10.1029/93jb03599

McAdoo, D. C., & Sandwell, D. T. (1985). Folding of oceanic lithosphere. *Journal of Geophysical Research*, *90*(B10), 8563–8569. https://doi.org/10.1029/jb090ib10p08563

Mitra, S., & Mount, V. S. (1998). Foreland basement-involved structures. *AAPG Bulletin*, *82*, 70–109. https://doi.org/10.1306/1d9bc39f-172d-11d7-8645000102c1865d

Moreno-Martín, D., Díez Fernández, R., de Vicente, G., Fernández, C., & Gómez Barreiro, J. (2022). Orogenic reworking and reactivation in Central Iberia: A record of Variscan, Permian and Alpine tectonics. *Tectonophysics*, *843*, 229601. https://doi.org/10.1016/j.tecto.2022.229601

Mouthereau, F., Deffontaines, B., Lacombe, O., & Angelier, J. (2002). Along-strike variations of the Taiwan belt front: Basement control on structural style, wedge geometry and kinematics. *Geological Society of America Bulletin*, *358*, 35–58.

Muñoz-Martín, A., de Vicente, G., Fernández-Lozano, J., Cloetingh, S., Willingshofer, E., Sokoutis, D., & Beekman, F. (2010). Spectral analysis of the gravity and elevation along the western Africa–Eurasia plate tectonic limit: Continental versus oceanic lithospheric folding signals. *Tectonophysics*, *495*(3), 298–314. https://doi.org/10.1016/j.tecto.2010.09.036

Narr, W., & Suppe, J. (1994). Kinematics of basement-involved compressive structures. *American Journal of Science*, *294*(7), 802–860. https://doi.org/10.2475/ajs.294.7.802

Pfiffner, O. A. (2017). Thick-skinned and thin-skinned tectonics: A global perspective. *Geosciences*, *7*(3), 71. https://doi.org/10.3390/geosciences7030071

Pfiffner, O. A., Mazzoli, S., & Butler, R. W. H. (2006). Thick-skinned and thin-skinned styles of continental contraction. In *Styles of continental contraction*. Geological Society of America.

Platt, J. P. (1993). Mechanics of oblique convergence. *Journal of Geophysical Research*, *98*(B9), 16239–16256. https://doi.org/10.1029/93jb00888

Price, N. J., & Cosgrove, J. W. (1990). *Analysis of geological structures* (p. 502). Cambridge University Press.

Ramberg, H. (1961). Contact strain and fold instability of a multilayered body under compression. *Geologische Rundschau*, *51*(2), 405–439. https://doi.org/10.1007/bf01820010

Ramsay, J. G. (1967). *Folding and fracturing of rocks* (p. 568). McGraw-Hill.

Regalla, C., Fisher, D., & Kirby, E. (2010). Timing and magnitude of shortening within the inner fore arc of the Japan Trench. *Journal of Geophysical Research*, *115*(B3). https://doi.org/10.1029/2009jb006603

Rubio Pascual, F. J. (2013). Evolución tectonotermal varisca del Sistema Central en Somosierra-Honrubia. *Nova Terra*, *44*, 1–364.

Rubio Pascual, F. J., Arenas, R., Catalán, J. R. M., Fernández, L. R. R., & Wijbrans, J. R. (2013). Thickening and exhumation of the Variscan roots in the Iberian central system: Tectonothermal processes and $^{40}Ar/^{39}Ar$ ages. *Tectonophysics*, *587*, 207–221. https://doi.org/10.1016/j.tecto.2012.10.005

Ruiz, J., Gómez-Ortiz, D., & Tejero, R. (2006). Effective elastic thicknesses of the lithosphere in the Central Iberian Peninsula from heat flow: Implications of the rheology of the continental lithospheric mantle. *Journal of Geodynamics*, *41*(5), 500–509. https://doi.org/10.1016/j.jog.2006.01.005

Schmalholz, S. M., Kaus, B. J. P., & Burg, J.-P. (2009). Stress-strength relationship in the lithosphere during continental collision. *Geology*, *37*(9), 775–778. https://doi.org/10.1130/g25678a.1

Schmidt, C. J., Genovese, P. W., & Chase, R. B. (1993). Role of basement fabric and cover-rock lithology on the geometry and kinematics of twelve folds in the Rocky Mountain foreland. In *Laramide basement deformation in the Rocky Mountain Foreland of the western United States* (pp. 1–44). Geological Society of America.

Selander, J., Oskin, M., Ormukov, C., & Abdrakhmatov, K. (2012). Inherited strike-slip faults as an origin for basement-cored uplifts: Example of the Kungey and Zailiskey ranges, northern Tian Shan. *Tectonics*, *31*(4). https://doi.org/10.1029/2011tc003002

So, B. D., Yuen, D. A., Regenauer-Lieb, K., & Lee, S. M. (2012). Asymmetric lithospheric instability facilitated by shear modulus contrast: Implications for shear zones. *Geophysical Journal International*, *190*(1), 23–36. https://doi.org/10.1111/j.1365-246x.2012.05473.x

Sokoutis, D., Burg, J. P., Bonini, M., Corti, G., & Cloetingh, S. (2005). Lithospheric-scale structures from the perspective of analogue continental collision. *Tectonophysics*, *406*(1–2), 1–15. https://doi.org/10.1016/j.tecto.2005.05.025

Sopeña, A., López, J., Arche, A., Pérez-Arlucea, M., Ramos, A., Virgili, C., & Hernando, S. (1988). Chapter 31—Permian and Triassic rift basins of the Iberian Peninsula. In W. Manspeizer (Ed.), *Developments in Geotectonics* (pp. 757–786). Elsevier.

Suriñach, E., & Vegas, R. (1988). Lateral inhomogeneities of the Hercynian crust in central Spain. *Physics of the Earth and Planetary Interiors*, *51*(1), 226–234. https://doi.org/10.1016/0031-9201(88)90049-0

Tesauro, M., Kaban, M. K., & Cloetingh, S. (2009). A new thermal and rheological model of the European lithosphere. *Tectonophysics*, *476*(3–4), 478–495. https://doi.org/10.1016/j.tecto.2009.07.022

Teyssier, C., & Whitney, D. L. (2002). Gneiss domes and orogeny. *Geology*, *30*(12), 1139–1142. https://doi.org/10.1130/0091-7613(2002)030<1139:gdao>2.0.co;2

Tikoff, B., Siddoway, C., Sokoutis, D., & Willingshofer, E. (2022). The lithospheric folding model applied to the Bighorn uplift during the Laramide orogeny. In J. P. Craddock, D. H. Malone, B. Z. Foreman, & A. Konstantinou (Eds.), *Tectonic evolution of the Sevier-Laramide Hinterland, thrust belt, and foreland, and postorogenic slab rollback (180–20 Ma)* (Vol. 555). Geological Society of America. https://doi.org/10.1130/2021.2555(08)

Turcotte, D. L., & Schubert, G. (2002). *Geodynamics*. Cambridge University Press.

Van Wees, J. D., Cloetingh, S., & de Vicente, G. (1996). The role of pre-existing faults in basin evolution: Constraints from 2D finite element and 3D flexure models. *Geological Society, London, Special Publications*, *99*(1), 297–320. https://doi.org/10.1144/gsl.sp.1996.099.01.22

Watts, A. B., & Burov, E. B. (2003). Lithospheric strength and its relationship to the elastic and seismogenic layer thickness. *Earth and Planetary Science Letters*, *213*(1–2), 113–131. https://doi.org/10.1016/s0012-821x(03)00289-9

Webb, L. E., & Johnson, C. L. (2006). Tertiary strike-slip faulting in southeastern Mongolia and implications for Asian tectonics. *Earth and Planetary Science Letters*, *241*(1–2), 323–335. https://doi.org/10.1016/j.epsl.2005.10.033

Withjack, M. O., Baum, M. S., & Schlische, R. W. (2010). Influence of preexisting fault fabric on inversion-related deformation: A case study of the inverted Fundy rift basin, southeastern Canada. *Tectonics*, *29*(6), TC6004. https://doi.org/10.1029/2010tc002744

Yin, A. (2004). Gneiss domes and gneiss dome systems. In D. L. Whitney, C. Teyssier, & C. S. Siddoway (Eds.), *Gneiss domes in orogeny* (pp. 1–14). Geological Society of America Special Paper. https://doi.org/10.1130/0-8137-2380-9.1